Probing the Dependence of Long-Range, Four-Atom Interactions on Intermolecular Orientation: 2. Molecular Deuterium and Iodine Monochloride†

Joshua P. Darr‡ and Richard A. Loomis*,§

Department of Chemistry, Washington University in St. Louis, One Brookings Drive, CB 1134, Saint Louis, Missouri 63130

Anne B. McCoy⊥

Department of Chemistry, The Ohio State University, Columbus, Ohio 43210

Received: April 4, 2008; Revised Manuscript Received: July 21, 2008

Laser-induced fluorescence and action spectroscopy experiments have identified multiple conformers of the $D_2\cdots ICl$ van der Waals complex for both *ortho*-D_2 (*o*-D_2) and *para*-D_2 (*p*-D_2). As with the analogous $H_2\cdots ICl$ van der Waals complexes [Darr, J. P.; Crowther, A. C.; Loomis, R. A.; Ray, S. E.; McCoy, A. B. *J. Phys. Chem. A* 2007, *111*, 13387], the C_{2v} conformer with the deuterium molecule localized at the iodine atom end of the dihalogen is significantly more stable than the asymmetric conformer that has the deuterium positioned orthogonally to the ICl bond axis, $D_0'' = 223.9(2.4)$ versus $97.3(8)-103.9(3)$ cm^{-1} for *p*-$D_2\cdots I^{35}Cl(X,v''=0)$. For both conformers, complexes containing *p*-D_2 are found to be more strongly bound than those with *o*-D_2. The electronically excited $D_2\cdots ICl(A,v')$ and $D_2\cdots ICl(B,v')$ complexes are found to have equilibrium geometries that are nearly the same as those of the ground-state asymmetric structures. Calculated $D_2\cdots ICl(B,v'=3)$ energies and probability amplitudes obtained using a simple scaled He + $ICl(B,v'=3)$ potential provide clues to the nature of the different excited-state levels accessed.

1. Introduction

We recently published results characterizing the long-range interactions of hydrogen, H_2, and the dihalogen iodine monochloride, ICl, hereafter referred to as Paper I.[1] These ongoing investigations are intended to extend the vast work undertaken on three-atom rare gas−dihalogen ($Rg\cdots XY$) van der Waals complexes to the four-atom regime, with the specific goal of more accurately characterizing multidimensional intermolecular potential energy surfaces (PESs). As reported in Paper I, spectroscopic features associated with two distinct, ground-state $H_2\cdots ICl(X,v'=0)$ conformers for both *ortho*-$H_2(j = 1)$ and *para*-$H_2(j = 0)$, abbreviated as *o*-H_2 and *p*-H_2, respectively, and both $I^{35}Cl$ and $I^{37}Cl$ isotopomers were observed in the ICl B−X and A−X regions. The equilibrium geometry of the more strongly bound conformer, with a ground-state binding energy of 186.4(3) cm^{-1}, was determined to have C_{2v} symmetry, with the H_2 moiety localized at the iodine end of the dihalogen, as illustrated in Figure 1. The C_{2v} conformer can be associated with the linear conformer of the $Rg\cdots XY$ complexes, where the Rg atom is localized at the end of the diatomic along the intermolecular axis well.[2−5] A rotational-contour fit of the feature associated with the other conformer, which is ≈100 cm^{-1} less strongly bound, led us to conclude that the H_2 subunit is localized in a well orthogonal to the dihalogen bond axis, resulting in an asymmetric equilibrium geometry, as shown in Figure 1. The asymmetric conformer can be associated with the T-shaped or near-T-shaped conformer of the $Rg\cdots XY$ complexes, where pairwise additive forces result in the Rg atom being localized in the minimum positioned orthogonally to the dihalogen axis.[2−5] In both of the $H_2\cdots ICl(X,v''=0)$ conformations, the orientation of H_2 within the complex was not experimentally determined.

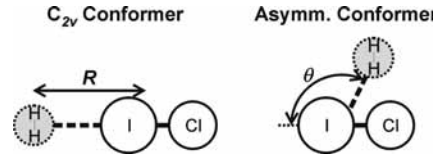

Figure 1. Equilibrium geometries of the C_{2v} and asymmetric $H_2\cdots ICl$ conformers characterized in Paper I.[1] The intermolecular distance is depicted as *R*, and the angle between the ICl bond axis and *R* is θ. The same geometries are found for the $D_2\cdots ICl$ isotopologues.

Assignments of the excited-state intermolecular vibrational levels accessed by transitions of the ground-state conformer were made by considering the calculated energy levels and probability amplitudes of the levels bound within the excited state. For clarity, we use the index n' to identify the different intermolecular vibrational energy levels, with $n' = 0$ being the most energetically stable. The $n' = 0$ level in the excited-state H_2 + $ICl(B,v')$ PES has nearly the same geometry as the asymmetric ground-state conformer and is accessed by rovibronic transitions of that conformer. The excited-state intermolecular vibrational levels accessed by rovibronic transitions of the ground-state C_{2v} conformer were assigned as states with the probability amplitude delocalized along the angular coordinate, $n' \geq 1$, with zero and one quanta of intermolecular stretching excitation. The qualitative agreement obtained between the energy levels experimentally accessed with those calculated using a modified He + $ICl(B,v'=3)$ PES[6] indicates that the intermolecular motions and energies are not sensitive to the details of the excited-state PES.

† Part of the "Stephen R. Leone Festschrift".

* To whom correspondence should be addressed. E-mail: loomis@wustl.edu.

‡ Present Address: JILA, University of Colorado, Campus Box 440, Boulder, Colorado 80309.

§ E-mail: loomis@wustl.edu.

⊥ E-mail: mccoy@chemistry.ohio-state.edu.

10.1021/jp802917f CCC: $40.75
Published on Web 08/15/2008

In this paper, we present results for complexes of *ortho*-D_2 ($j = 0$) and *para*-D_2($j = 1$), abbreviated as *o*-D_2 and *p*-D_2, respectively, with ICl that complement those in Paper I. The greater mass of D_2 in comparison to that of H_2 results in a decreased zero-point energy and an increase in the number of bound intermolecular vibrational levels. Binding energies of the ground- and excited-state *o*-D_2···ICl and *p*-D_2···ICl complexes are experimentally measured. Unexpectedly, multiple excited-state intermolecular vibrational levels are accessed by transitions of the asymmetric *o*-D_2···$I^{35}Cl(X,v''=0)$ complex; transitions to similar levels were not observed for the asymmetric *p*-D_2···$I^{35}Cl(X,v''=0)$ or *o*,*p*-H_2···$I^{35}Cl(X,v''=0)$ complexes. The modified He + ICl(B,$v'=3$) PES is used to calculate the bound D_2···$I^{35}Cl(B,v'=3)$ intermolecular vibrational levels and probability amplitudes. As in Paper I, we have assumed that the intermolecular potential is rather isotropic, and the hydrogen molecule is treated as a spherical object; as such, differences in the interactions of complexes containing *o*-D_2 and *p*-D_2 are not predicted.

2. Experimental Methods

The D_2···ICl(X,$v'=0$) van der Waals complexes were stabilized, and laser-induced fluorescence (LIF) and action spectra of the complexes were recorded in a manner completely analogous to that described in Paper I and are only briefly discussed here. A pulsed supersonic expansion of ICl entrained in a mixture of D_2 in He with a backing pressure of 7.9 bar was used to stabilize the ground-state complexes. Varying concentrations of normal-deuterium (*n*-D_2), consisting of a 2:1 ratio of *o*-D_2 with $j = 0$ to *p*-D_2 with $j = 1$, were utilized. A carrier gas consisting of a predominantly *o*-D_2 composition in helium was also used. Spectra were recorded at varying downstream distances to interrogate different temperature regimes and changes in the relative populations of the conformers. LIF spectra were recorded in the ICl B−X, $v'-0$ and A−X, $v'-0$ regions, 17 450−18 100 and 16 450−17 000 cm^{-1}, respectively, using a pulsed nanosecond Nd:YAG-pumped dye laser. Action spectra were recorded by scanning a pump laser in wavelength through the same spectral regions and probing $I^{35}Cl(B,v')$ and $I^{35}Cl(A,v')$ dissociation products using a second Nd:YAG-pumped dye laser that was fixed on either an $I^{35}Cl$ E−B, $v^{\dagger}-v'$ or β−A, $v^{\dagger}-v'$ rovibronic transition, in the region between 22 750 and 23 200 cm^{-1} [7−10] and delayed in time from the pump laser. In this manner, spectra associated with transitions of species specifically containing the $I^{35}Cl$ isotopologue were obtained by collecting fluorescence from either the $I^{35}Cl(E,v^{\dagger})$ or $I^{35}Cl(\beta,v^{\dagger})$ ion pair states that was induced by the probe laser.

3. Results and Discussion

A. Survey LIF and Action Spectra. As shown in Figure 2a, numerous LIF features are observed throughout the $I^{35,37}Cl$ B−X, 2−0 and 3−0 spectral regions. In addition to the monomer bands, which are identified with asterisks, features associated with transitions of the T-shaped and linear He···$I^{35,37}Cl(X,v'0)$ complexes,[2,11−14] which are marked with daggers, are also detected. The remaining fluorescence signals are attributed to transitions of *o*,*p*-D_2···$I^{35,37}Cl(X,v''=0)$ complexes to bound or dissociative states correlating with the $D_2(j = 0,1)$ + ICl(B,$v'=2,3$) potentials. In order to assist in the assignments of these additional LIF signals, two-laser action spectroscopy experiments were performed.

Figure 2b contains an action spectrum recorded with the probe laser fixed on the $I^{35}Cl$ E−B, 10−1 transition and the same source conditions utilized when recording the LIF spectrum shown in Figure 2a. This action spectrum should preferentially contain discrete features associated with transitions to D_2···$I^{35}Cl(B,v'=3)$ or D_2···$I^{35}Cl(B,v'=2)$ intermolecular vibrational levels that undergo $\Delta v = -2$ or -1 vibrational predissociation, respectively. The results presented in Paper I indicate that continuum signals associated with transitions of the ground-state C_{2v} conformer to the inner repulsive wall above the D_2 + $I^{35}Cl(B,v'=1)$ dissociation limit can also be observed in this action spectrum. The assignments of the features in this and similar spectra acquired using D_2 in He carrier gases are based largely on comparisons with the results presented in Paper I, although systematic checks and comparisons with theory are made to verify the assignments. The transition energy, the wavenumber shift from the corresponding $I^{35}Cl$ band origin, and the ground-state conformer or molecule associated with each observed feature are included in Table 1.

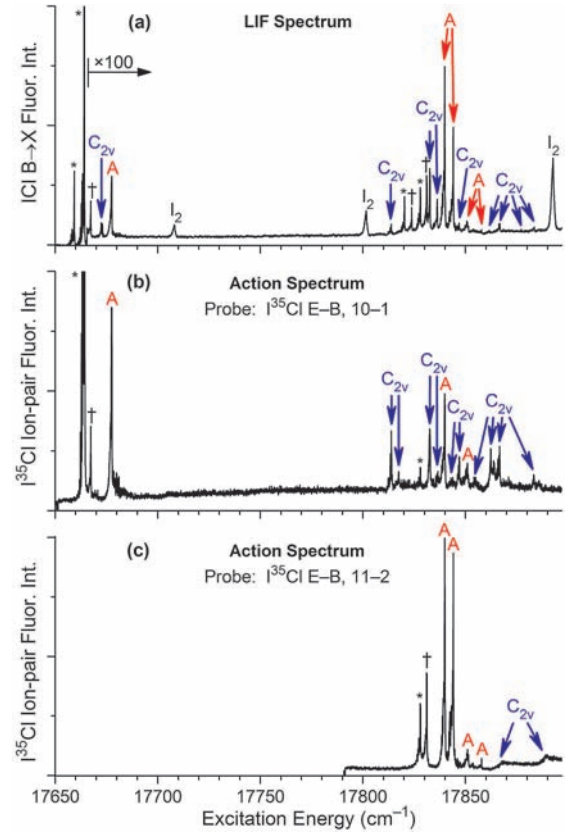

Figure 2. Laser-induced fluorescence (LIF) and action spectra acquired in the ICl B−X, 2−0 and 3−0 spectral regions. Panel (a) contains an LIF spectrum, and (b) and (c) contain action spectra obtained with the probe laser fixed on the indicated $I^{35}Cl$ E−B, $v^{\dagger}-v'$ transitions. The bare $I^{35,37}Cl$ and He···$I^{35,37}Cl$ transitions are marked by asterisks and daggers, respectively, in this and the following figures. Trace I_2 contamination was also observed in the LIF spectrum, and these features are identified. Features associated with transitions of the asymmetric and C_{2v} D_2···ICl(X,$v''=0$) conformers are labeled with A and C_{2v}, respectively. Note the scale change in panel (a) just to higher energy than the very intense $I^{35,37}Cl$ B−X, 2−0 features.

The most intense feature in this action spectrum is observed at 17 677.5 cm^{-1}, 13.4 cm^{-1} above the $I^{35}Cl$ B−X, 2−0 band origin, and is associated with transitions of the ground-state asymmetric conformer. Several additional discrete bands are observed to higher transition energies that are attributed to transitions of the C_{2v} D_2···$I^{35}Cl(X,v''=0)$ conformer. A very weak continuum signal is also observed in this spectrum, beginning at 17 704 cm^{-1} and extending to higher transition

TABLE 1: The Transition Energies and Shifts from the $I^{35}Cl$ B−X, 2−0 and 3−0 Monomer Band Origins (in cm^{-1}) of the Peaks of the Observed $D_2\cdots I^{35}Cl$ Features[a]

peak	shift	assignment 2−0	peak	shift	assignment 3−0
17 664.1	0	$I^{35}Cl$	17 827.5	0	$I^{35}Cl$
17 677.5	13.4	asymmetric	17 839.9	12.4	asymmetric *o*-$D_2\cdots I^{35}Cl$
		o,*p*-$D_2\cdots I^{35}Cl$	17 844.1	16.6	asymmetric *p*-$D_2\cdots I^{35}Cl$
			17 850.7	23.2	asymmetric *o*-$D_2\cdots I^{35}Cl$
			17 857.9	30.4	asymmetric *o*-$D_2\cdots I^{35}Cl$
17 813.8	149.7	C_{2v} *o*-$D_2\cdots I^{35}Cl$	17 976.4	148.9	C_{2v} *o*-$D_2\cdots I^{35}Cl$
17 817.4	153.3	C_{2v} *o*-$D_2\cdots I^{35}Cl$	17 981.0	153.5	C_{2v} *o*-$D_2\cdots I^{35}Cl$
			17 984.8	157.3	C_{2v} *o*-$D_2\cdots I^{35}Cl$
17 832.6	168.5	C_{2v} *p*-$D_2\cdots I^{35}Cl$	17 995.4	167.9	C_{2v} *p*-$D_2\cdots I^{35}Cl$
			18 001.5	174	C_{2v} *p*-$D_2\cdots I^{35}Cl$
17 846.9	182.8	C_{2v} *o*-$D_2\cdots I^{35}Cl$	18 010.0	182.5	C_{2v} *o*-$D_2\cdots I^{35}Cl$
			18 014.1	186.6	C_{2v} *o*-$D_2\cdots I^{35}Cl$
			18 019.1	191.6	C_{2v} *o*-$D_2\cdots I^{35}Cl$
17 862.3	198.2	C_{2v} *p*-$D_2\cdots I^{35}Cl$	18 030.1	202.6	C_{2v} *p*-$D_2\cdots I^{35}Cl$
17 866.7	202.6	C_{2v} *p*-$D_2\cdots I^{35}Cl$	18 033.5	206	C_{2v} *p*-$D_2\cdots I^{35}Cl$
17 883.5	219.4	C_{2v} *p*-$D_2\cdots I^{35}Cl$	18 046.5	219	C_{2v} *p*-$D_2\cdots I^{35}Cl$
17 885.9	221.8	C_{2v} *p*-$D_2\cdots I^{35}Cl$	18 049.1	221.6	C_{2v} *p*-$D_2\cdots I^{35}Cl$

[a] The assignments correspond to the ground-state conformers associated with the features.

energies; this continuum signal is associated with transitions of the C_{2v} conformer to the inner repulsive wall above the $D_2 + I^{35}Cl(B,v'=1)$ asymptote. The remaining discrete bands are observed at higher energies, near the $I^{35}Cl$ B−X, 3−0 band origin at 17 827.5 cm^{-1}. On the basis of these data, it is not certain whether the excited-state levels associated with these bands are bound within the $D_2 + ICl(B,v'=2)$ or $D_2 + ICl(B,v'=3)$ potentials.

In order to distinguish between these two possibilities, we acquired an action spectrum through the same region with the probe laser fixed on the $I^{35}Cl$ E−B, 11−2 transition, shown in Figure 2c. There are no discrete $D_2\cdots I^{35}Cl$ features observed at energies lower than the $I^{35}Cl$ B−X, 3−0 band origin when probing the $I^{35}Cl(B,v'=2)$ fragments. At slightly higher energies, though, there are two intense and two weaker discrete features. All of these bands are associated with transitions of the asymmetric, ground-state $D_2\cdots I^{35}Cl(X,v''=0)$ conformer to intermolecular vibrational levels within the $D_2 + ICl(B,v'=3)$ PES. The features at 17 839.9 and 17 850.7 cm^{-1} are observed in Figure 2b and c, and the excited-state levels accessed undergo vibrational predissociation into both the $\Delta v = -1$ and -2 channels. The levels accessed in the other two bands, at 17 844.1 and 17 857.9 cm^{-1}, only dissociate through the $\Delta v = -1$ channel. As mentioned in Paper I, a curve crossing dictates that only $ICl(B,v')$ molecular vibrational levels with $v' \leq 3$ are bound,[15] and as a result, these features cannot be associated with transitions to $D_2\cdots I^{35}Cl(B,v'=4)$ intermolecular levels that undergo $\Delta v = -2$ vibrational predissociation. The remaining discrete features observed at higher energies in Figure 2b are associated with transitions of the C_{2v} ground-state $D_2\cdots I^{35}Cl(X,v''=0)$ conformer to vibrationally excited levels within the $D_2 + I^{35}Cl(B,v'=2)$ intermolecular PES. Lastly, the two continuum signals, which begin at 17 863 and 17 885 cm^{-1} and extend to higher transition energies, are attributed to direct dissociation of $D_2\cdots I^{35}Cl$ complexes promoted to the repulsive region of the intermolecular potential above the $D_2 + ICl(B,v'=2)$ dissociation limit. The shifts of the onsets of these continuum signals to higher energy than those of the $I^{35}Cl$ B−X, 2−0 band origin are 199 and 221 cm^{-1}, and the transitions are associated with the C_{2v} $D_2\cdots I^{35}Cl(X,v'0)$ conformer.

B. Signal Dependence on Source Conditions. Since the relative populations of the $D_2\cdots ICl(X,v''=0)$ conformers do not necessarily follow Boltzmann statistics, we do not estimate the populations and the relative energies of the conformers using rotational or vibrational temperatures. An accurate determination of the actual populations of the two $D_2\cdots ICl(X,v''=0)$ conformers using the spectra is also not possible without accurate Franck−Condon factors for transitions of both conformers. Since the rotational contours of the asymmetric $D_2\cdots ICl$ features strongly resemble those of the T-shaped $Rg\cdots XY$ features,[2−5] it seems likely that these $D_2\cdots ICl$ transitions are vertical with little change in geometry. In contrast, since the higher-energy features are associated with transitions of the rigid C_{2v} conformer to delocalized intermolecular vibrational levels, the probabilities for these transitions are presumed to be significantly smaller. Therefore, in order to identify which conformer is energetically more stable and to further characterize the properties of the conformers contributing to the LIF and action spectra, we examined how the relative intensities of the different $D_2\cdots I^{35}Cl$ features changed with variations in the source conditions utilized in the supersonic expansion.

The middle trace in Figure 3 is an action spectrum acquired with the probe laser fixed on the $I^{35}Cl$ E−B, 11−2 transition and scanning the pump laser to higher energies than the $I^{35}Cl$ B−X, 3−0 region. This spectrum was acquired using a 5% D_2 in He carrier gas. The intensity of the lower-energy feature at 17 839.9 cm^{-1} is approximately seven times higher than the most intense of the higher-energy features at 17 976.4 cm^{-1} when subtracting off the continuum background signal. The upper trace shows the same action spectrum, only recorded with a 10% *n*-D_2 in He carrier gas. In this spectrum, the relative intensity of the feature at 17 976.4 cm^{-1} has increased and is now only a factor of four to five times weaker than the feature at 17 839.9 cm^{-1}. The intensity of the higher-energy feature at 17 995.4 cm^{-1} has increased even more, and it is now more intense than the feature at 17 976.4 cm^{-1}.

The spectra of several $Rg\cdots XY$ complexes recorded with varying expansion conditions[2−4,12] revealed similar tendencies as observed here; the intensity of the higher-energy feature associated with transitions of the energetically more stable linear $Rg\cdots XY$ conformer increases relative to that of the lower-energy feature, which is associated with transitions of the T-shaped $Rg\cdots XY$ conformer, with cooling and additional collisions along the expansion. The population transfer of the $Rg\cdots XY$ conformers is associated with either collisional isomerization or an exchange mechanism.[2,16] In the second

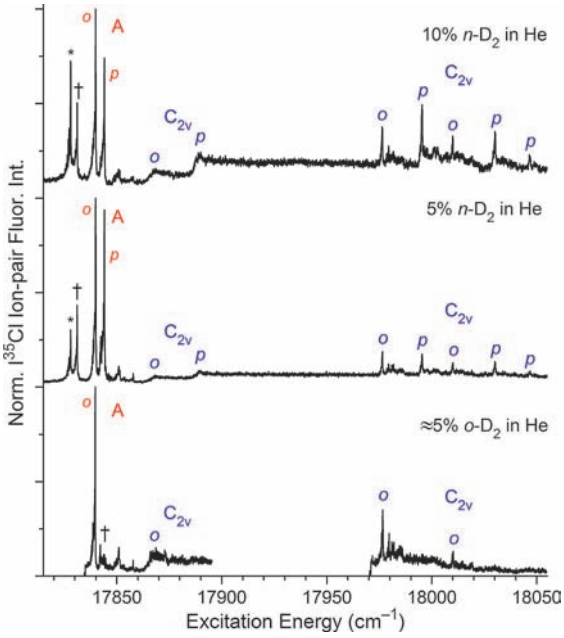

Figure 3. Action spectra recorded in and above the ICl B−X, 3−0 region using different source conditions. The top and middle spectra were acquired with 10 and 5% n-D_2 in He carrier gas mixtures, respectively. The bottom spectrum was acquired using a 5% o-D_2 in He carrier gas. Features associated with transitions of the asymmetric and C_{2v} $D_2\cdots ICl(X,v''=0)$ conformers are labeled with A and C_{2v}, and those containing o-D_2 and p-D_2 are identified with o and p, respectively.

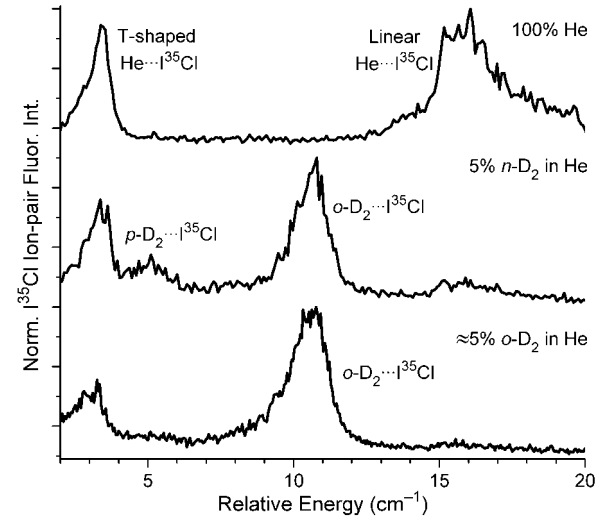

Figure 4. Action spectra recorded in the $I^{35}Cl$ A−X, 19−0 spectral region while probing the $I^{35}Cl$ β−A, 4−18 transition at 23 115 cm^{-1}.[9] The spectra are plotted as a function of transition energy relative to the $I^{35}Cl$ A−X, 19−0 band origin at 16 552.71 cm^{-1}.[8] The top spectrum was recorded using a pure He carrier gas, the middle spectrum was recorded using a 5% n-D_2 in He carrier gas, and the bottom spectrum was acquired with a 5% o-D_2 in He carrier gas. Similar spectra were taken in each of the $I^{35}Cl$ A−X, v'−0 regions included in Figure 5 in order to definitively identify the observed $D_2\cdots I^{35}Cl$ features.

mechanism, carrier gas atoms collide with a complex, occupy a minimum region of the intermolecular potential, and eject an atom initially localized in a higher-energy state of the complex. Since there is a significant potential barrier along the angular coordinate between the minima for the T-shaped and linear levels and the probability amplitudes for each level are localized in that region, these levels resemble distinct conformers of the ground-state complex.

Here, the increase in the concentration of D_2 molecules in the carrier gas enables further cooling of the $D_2\cdots ICl(X,v''=0)$ complexes via collisions that result in exchange events and in an increase in the relative population of the energetically more stable conformer. The ground-state complexes associated with the lower-energy features near the $I^{35}Cl$ B−X, 2−0 and 3−0 band origins are presumably the asymmetric conformers and are not as strongly bound as the C_{2v} ground-state conformers, which are associated with the features observed at higher transition energies.

Additional spectra were acquired using a carrier gas comprised of 5% nearly pure o-D_2 in He to compare and contrast with the spectra obtained using 5% n-D_2 in He so that those features associated with complexes containing o-D_2 and p-D_2 molecules could be determined. The o-D_2 in He spectrum, shown in the lower spectrum in Figure 3, is dramatically different than the two uppermost traces, which were acquired using n-D_2 in He. The discrete feature at 17 844.1 cm^{-1} is not observed when using o-D_2; the feature that is observed at nearly the same energy is shifted slightly and is associated with transitions of the linear $He\cdots I^{35}Cl(X,v''=0)$ conformer. The discrete features at 17 995.4, 18 001.5, 18 030.1, 18 033.5, 18 046.5, and 18 049.1 cm^{-1} and the continuum signal beginning at 17 885 cm^{-1} are also not observed when using the o-D_2 in He carrier gas. All of these bands are therefore associated with transitions of p-$D_2\cdots I^{35}Cl(X,v''=0)$ complexes. The signals that are observable in the lower trace, namely, the continuum at 17 863 cm^{-1}, the three discrete lower-energy features, and the six higher-energy features are associated with transitions of the o-$D_2\cdots I^{35}Cl(X,v''=0)$ complex. Furthermore, the lower-energy features correspond to transitions of the asymmetric $D_2\cdots I^{35}Cl(X,v''=0)$ conformer, while the continuum and discrete signals at higher energies correspond to transitions of the C_{2v} ground-state $D_2\cdots I^{35}Cl(X,v''=0)$ complex.

C. Binding Energies. The onset of the two continuum signals observed in the LIF and action spectra recorded in the ICl B−X, 3−0 region can be used to accurately determine the binding energies of the C_{2v}, ground-state o- and p-$D_2\cdots I^{35}Cl(X,v''=0)$ complexes.[1,17,18] As stated, these continuum signals are attributed to transitions of the C_{2v} ground-state conformers to the continuum of repulsive states above the $D_2 + I^{35}Cl(B,v'=2)$ intermolecular asymptote. In order to quantitatively set D_0', we use the mean value of the onset of the continuum and the peak of the continuum. The D_0' values are set as 202(3) and 223.9(2.4) cm^{-1} for the C_{2v} o- and p-$D_2\cdots I^{35}Cl(X,v''=0)$ conformers, respectively.

In order to estimate the binding energies of the asymmetric o- and p-$D_2\cdots I^{35}Cl(X,v''=0)$ complexes, for which no continuum signals are observed, we have recorded action spectra in consecutive ICl A−X, v'−0 regions to identify when the anharmonicity of the ICl(A) potential energetically closes the $\Delta v = -1$ vibrational predissociation channel.[19] Due to the large vibrational frequency and the small number of bound vibrational levels in the ICl(B) state,[15] it was necessary to record these spectra in the ICl A−X, v'−0 region despite the decrease of spectral resolution in the observed features that results from efficient vibrational predissociation. Figure 4 contains action spectra recorded in the $I^{35}Cl$ A−X, 19−0 spectral region with the probe laser fixed on the $I^{35}Cl$ β−A, 4−18 transition. The spectra are plotted relative to the $I^{35}Cl$ A−X, 19−0 monomer band origin at 16 552.71 cm^{-1}.[8] In order to definitively assign the o- and p-$D_2\cdots I^{35}Cl$ features, the spectra were acquired using different carrier gases. The top spectrum was acquired with a pure He carrier gas in order to identify the linear and T-shaped

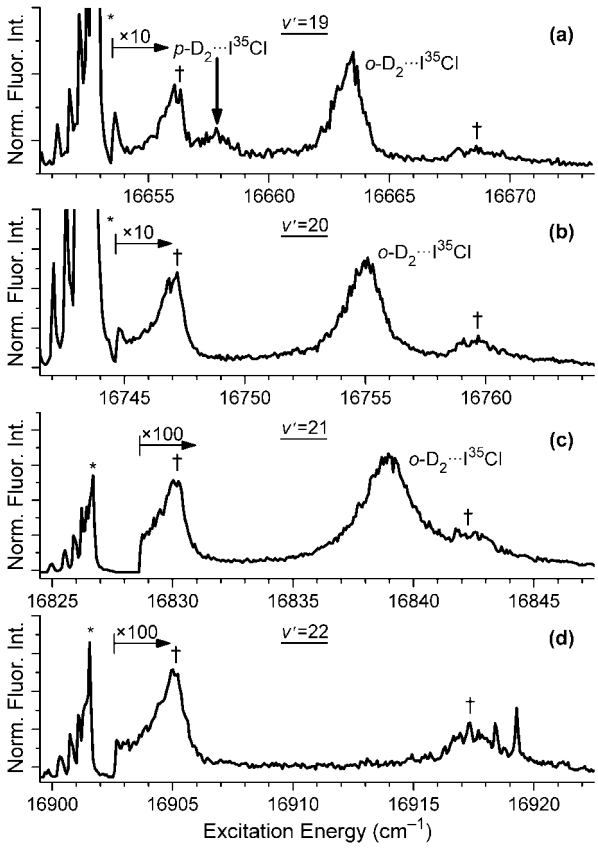

Figure 5. Action spectra recorded in consecutive ICl A−X, $v'-0$ spectral regions with the probe laser fixed on $I^{35}Cl$ $\beta-A$, $v^{\dagger}-v'$ transitions suitable to probe $\Delta v = -1$ $I^{35}Cl(A,v')$ vibrational predissociation products. The p-$D_2\cdots I^{35}Cl$ and o-$D_2\cdots I^{35}Cl$ features are labeled. The intensity scales are increased by the indicated amounts to higher energies than each of the monomer transitions.

$He\cdots I^{35}Cl$ A−X, 19−0 features. These features are observed at ≈3.4 and 16 cm^{-1}, respectively. When a 5% n-D_2 in He carrier gas is used, middle spectrum, two new features are observed that can be attributed to transitions of $D_2\cdots I^{35}Cl$ complexes in the ICl A−X, 19−0 region. A comparison with the bottom spectrum, acquired with a 5% o-D_2 in He carrier gas, shows that the feature at 5.1 cm^{-1} can be associated with transitions of a p-$D_2\cdots I^{35}Cl(X,v''=0)$ complex, while the feature at 10.8 cm^{-1} is attributed to o-$D_2\cdots I^{35}Cl$ transitions. Note that the energetic ordering of the p- and o-$D_2\cdots I^{35}Cl$ features is reversed in this spectral region in comparison with that in the ICl B−X, 3−0 region. Similar spectra were recorded for all of the regions over which action spectra were acquired to identify the energetic closing of the $\Delta v = -1$ vibrational predissociation channels.

Figure 5 contains action spectra acquired by scanning the pump laser throughout different ICl A−X, $v'-0$ regions with the probe laser fixed in wavelength to detect $ICl(A,v'-1)$ products. The spectrum in panel (a) was obtained by scanning the pump laser through the ICl A−X, 19−0 region with the probe laser fixed on the $I^{35}Cl$ $\beta-A$, 4−18 transition. Both o- and p-$D_2\cdots I^{35}Cl$ features are present, implying that the $\Delta v = -1$ vibrational predissociation channel is open for both of the excited-state complexes. The action spectrum in panel (b) was recorded in the ICl A−X, 20−0 region. Here, the $\Delta v = -1$ vibrational predissociation channel is open for the o-$D_2\cdots I^{35}Cl$ complex, but it is closed for p-$D_2\cdots I^{35}Cl$. The spectra in panels (c) and (d) indicate that the $\Delta v = -1$ vibrational predissociation channel is open for o-$D_2\cdots I^{35}Cl$ in the ICl A−X, 21−0 region but is closed in the ICl A−X, 22−0 region, respectively. Using the energies of the $I^{35}Cl(A,v')$ levels,[8] limits on the excited-state binding energies, D_0', of the p-$D_2\cdots I^{35}Cl(A,v'=19,20)$ levels can be established, $90.9 \le D_0' \le 98.8$ cm^{-1}. Similarly, the limits on the binding energies of the o-$D_2\cdots I^{35}Cl(A,v'=21,22)$ levels are $74.9 \le D_0' \le 82.9$ cm^{-1}. On the basis of the spectral shifts of the features in the action spectra to higher energies than the respective $I^{35}Cl$ A−X, $v'-0$ monomer transitions, the ground-state binding energies, D_0'', for the asymmetric conformers are $97.3(8) \le D_0'' \le 103.9(3)$ cm^{-1} for p-$D_2\cdots I^{35}Cl(X,v''=0)$ and $87.7(3) \le D_0'' \le 95.2(2)$ cm^{-1} for o-$D_2\cdots I^{35}Cl(X,v''=0)$. These D_0'' values are less than half pf those for the more strongly bound C_{2v} ground-state conformer, as suggested by the D_2/He carrier gas concentration dependence. The binding energies of the different complexes are listed in Table 2 for comparison.

It is desirable to develop trends for predicting intermolecular binding energies for three- or four-atom complexes with similar geometries based on expected electrostatic interactions. As reviewed in Paper I, the preferred geometries for complexes containing hydrogen and numerous diatomics appear to be dictated by electrostatic interactions. For diatomics with small quadrupole moments, CN (≈0.4)[20] and NH (≈0.46),[21] the $H_2\cdots NC$ [20,22] and $H_2\cdots NH$[21] complexes were found to have linear geometries. In this orientation, the electrostatic interactions are weak, and the intermolecular distances are fairly long. In contrast, for diatomics with larger quadrupole moments, OH (1.39 au),[23] HF (1.75 au),[24] HCl (2.8 au),[24] and ICl (>2 au),[25,26] the corresponding complexes with H_2 have been found to each have a C_{2v} equilibrium geometry in the ground electronic state.[1,27−29] The o-H_2 (or p-D_2) moiety in these complexes resembles a propeller motion with the $j = 1$ rotational angular momentum projected onto the internuclear axis. Therefore, the nodal structure in this orientation permits the H_2 (or D_2) molecule to access shorter intermolecular distances, thereby increasing the intermolecular interaction.

The binding energies of OH, HF, HCl, and ICl with He, Ne, H_2, and D_2 partners are included in Table 3; the geometries of these complexes are those with the partner localized in the linear well relative to the spectroscopically active partner. Despite the apparent role of electrostatic interactions in dictating the preferred geometries of these complexes, the well-characterized, long-range electrostatic interactions, including dipole−dipole, dipole−quadrupole, quadrupole-quadrupole, and dispersion

TABLE 2: Experimental Binding Energies (in cm^{-1}) of $D_2\cdots I^{35}Cl$ Complexes Determined in This Work and of $H_2\cdots I^{35}Cl$ Complexes (from ref 1) in Different ICl Electronic States

	C_{2v} X, $v''=0$	asymm. X, $v''=0$	A, v'	B, $v'=3$
o-$H_2(j = 1)$	186.4(3)	82.8(3)−89.6(3)	73.7(4)−80.5(4) [a]	69.5(3)−76.3(3)
p-$H_2(j = 0)$	156.8(1.3)	70.0(1)−77.9(3)	59.2(2)−67.1(4) [a]	59.4(1)−67.3(3)
p-$D_2(j = 1)$	223.9(2.4)	97.3(8)−103.9(3)	92.2(9)−98.8(4) [b]	81.2(8)−87.8(3)
o-$D_2(j = 0)$	202(3)	87.7(3)−95.2(2)	76.9(4)−84.4(3) [b]	75.8(3)−83.3(2)

[a] Values are for $ICl(A,v'=23)$. [b] Values are for $ICl(A,v'=19)$.

forces,[30] cannot be used to reproduce the observed relative binding energies of the different complexes. It is most likely the role of zero-point energy and the slight differences in the anisotropies of the intermolecular PESs that can significantly influence the binding energies of these weakly bound systems. As an aside, we find it surprising that the trends for binding energies in the OH family of complexes are most similar to those of the ICl systems; the binding energies increase by factors of 4−5 when substituting Ne for He, of 8−9 when substituting o-H_2($j = 1$) for He, and of 10−11 when substituting p-D_2-($j = 1$) for He.

As noted in Table 2, the binding energies of the asymmetric conformers of the $H_2\cdots ICl(X,v''=0)$ and $D_2\cdots ICl(X,v''=0)$ complexes are significantly lower than the corresponding C_{2v} conformers; the binding energy of the asymmetric conformer is ≈44% that of the C_{2v} conformer for all four complexes. We find it particularly surprising that there is not a noticeable dependence of the relative binding energies on the rotational angular momentum of the hydrogen molecule within the asymmetric conformers. We conclude that for the hydrogen in this T-shaped potential well relative to the ICl molecule, the potential is rather isotropic with respect to the H_2 and D_2 bending motions, and the hydrogen molecules behave as free internal rotors in the asymmetric conformers.

D. $D_2\cdots I^{35}Cl(B,v'=3)$ Intermolecular Vibrational Levels. The transition energies of the o- and p-$D_2\cdots I^{35}Cl$ features and the binding energies of the ground-state conformers are used to generate an energy level diagram, shown in Figure 6, to aid in assigning the observed features and to compare and contrast the interactions of the different conformers. The energies of the C_{2v} (blue) and asymmetric (red) ground-state o- and p-$D_2\cdots I^{35}Cl(X,v''=0)$ conformers are depicted, as are the energies of the excited-state levels accessed by transitions of each. The breadth of the boxes for the asymmetric ground-state and lowest-lying excited-state levels indicate the uncertainty in the energies of the levels. Note also the change in scale for the ground- and excited-state regions.

The lowest-lying p-$D_2\cdots I^{35}Cl(B,v'=3)$ level with no intermolecular vibrational excitation, $n' = 0$, lies between −80.7 and −87.3 cm^{-1} relative to the D_2 + ICl(B,v'=3) dissociation limit. The features accessed by transitions of the C_{2v} conformer at higher energies have congested contours and most likely consist of transitions to multiple intermolecular vibrational levels. For instance, the weak p-$D_2\cdots I^{35}Cl$ feature at 18 001.5 cm^{-1} appears to be a satellite of the feature at 17 995.4 cm^{-1}, as observed in the top spectrum in Figure 3. These levels are at −56.1 and −50.0 cm^{-1} with respect to the asymptote. There is a significant gap until the next intermolecular vibrational levels, which are also accessed by transitions of the C_{2v} conformer. These higher-lying p-$D_2\cdots I^{35}Cl(B,v'=3)$ intermolecular levels lie just below the dissociation limit, −21.4, −18.0, −5.0, and −2.4 cm^{-1}. The properties of these excited-state intermolecular vibrational levels and the regions of the multidimensional PES that are sampled by them are not obvious based solely on the energetics of the features.

The energy level pattern for the excited-state o-$D_2\cdots I^{35}Cl(B,v'=3)$ intermolecular vibrational levels is even more complicated than that for p-$D_2\cdots I^{35}Cl(B,v'=3)$. Just above the lowest-lying level, $n' = 0$, there are two additional levels that are also accessed by transitions of the asymmetric o-$D_2\cdots I^{35}Cl(X,v''=0)$ conformer. It is not currently understood why transitions to similar levels are not observed for the p-$D_2\cdots I^{35}Cl$ or o,p-$H_2\cdots I^{35}Cl$ complexes. To higher energy, there is a gap over which no levels are observed; then, at even higher energies, there are numerous o-$D_2\cdots I^{35}Cl(B,v'=3)$ intermolecular vibrational levels that are accessed by transitions of the C_{2v} ground-state conformer.

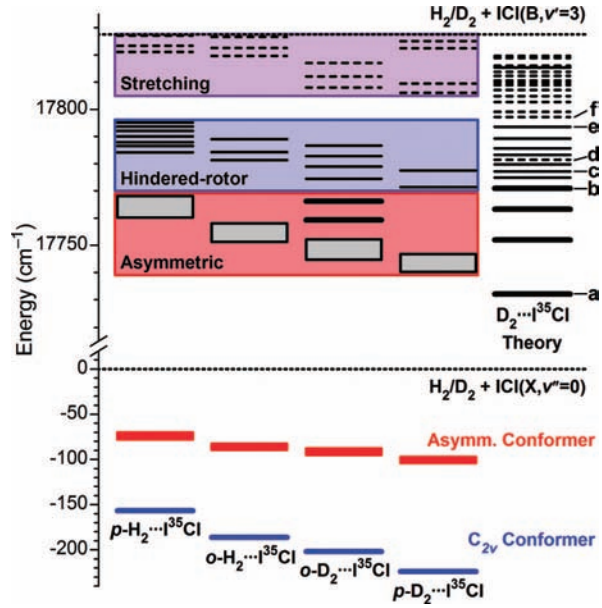

Figure 6. An energy-level diagram of the bound o,p-H_2/$D_2\cdots I^{35}Cl(X,v''=0)$ and o,p-$H_2/D_2\cdots I^{35}Cl(B,v'=3)$ intermolecular vibrational levels observed experimentally. The energies of the $H_2\cdots I^{35}Cl$ levels are from ref 1. The calculated $D_2\cdots I^{35}Cl(B,v'=3)$ levels are included on the right for comparison; those levels labeled with letters are plotted in the corresponding panels in Figure 7. In the ground state, thick blue lines indicate energies of the rigid C_{2v} conformers, and red boxes indicate the energies of the asymmetric conformers. In the excited state, the boxes indicate the energies of the lowest energy level with an asymmetric geometry. The energy breadths of the boxes indicate the uncertainty of the asymmetric levels. The thin lines and dashed lines indicate excited-state levels that resemble hindered rotor levels and hindered rotor levels with intermolecular stretching excitation, respectively. The red shading indicates the region of the excited-state potential in which the levels have asymmetric geometries. The blue shading indicates the region over which the levels are delocalized in the angular coordinate, representing hindered rotor levels. The purple shading represents levels that may have stretching excitation in addition to being delocalized. The dissociation limits in the ground and excited states are indicated with dotted lines.

TABLE 3: Comparison of the Binding Energies (in cm^{-1}) of X···ICl, X···HCl, and X···HF Complexes, with X = He, Ne, o-H_2, p-H_2, p-D_2, and o-D_2, Localized in the Linear Well with Respect to the ICl, HCl, and HF Partner

	OH	HF	HCl	ICl
He	≈6[33]	7.1(1)[34]	10.1(1.2)[34]	22.0(2)[2]
Ne	29.0[35]	≈38[36]	30.7[37]	84(1)[4]
o-H_2($j = 1$)	54[38]	70.6[27]	45(2)[29]	186.4(3)[1]
p-H_2($j = 0$)	−	−	≈33[29]	156.8(1.3)[1]
p-D_2($j = 1$)	66[38]	95[39]	−	223.9(2.4)
o-D_2($j = 0$)	−	76[39]	−	202(3)

Calculations of the excited-state $D_2\cdots I^{35}Cl(B,v'=3)$ intermolecular vibrational energies and probability amplitudes were performed to investigate the nature of the states that are accessed in these experiments. In our previous study on $H_2\cdots I^{35}Cl(B,v'=3)$, we obtained an approximate PES by assuming that the H_2 was spherical and scaling the He + $I^{35}Cl(B,v'=3)$ PES to yield the experimental binding energy. We were motivated to do this by the conclusion drawn in earlier studies on $He\cdots ICl(B,v')$,[2,6] $He\cdots Br_2(B,v')$,[3] and $He\cdots I_2(B,v')$,[31] where we showed that the most important parameters in the B state PES are the dissociation energy and the barrier to free

rotation of the dihalogen. Although small changes in the intermolecular potential might be expected upon deuterium substitution,[32] given the approximate nature of the B state PES used in this study, we utilized the same H_2 + ICl(B,v'=3) PES in these D_2···ICl(B,v') calculations as we previously used in our investigation of H_2···ICl(B,v').

In these calculations, we treat the hydrogen molecule as a spherical object, which is probably a good assumption for *o*-D_2-(j = 0) if mixing with other j rotor states, lying to significantly higher energy, is small. We recognize that this assumption is not representative of *p*-D_2(j = 1) interacting with ICl. Calculations of the H_2 + HCl interactions indicate that the anisotropy of the PES along the H_2 bend coordinate does indeed localize the hydrogen atoms in a C_{2v} geometry via mixing with higher j states.[29] This localization of the H_2 rotational probability amplitude leads to a noticeably higher energy for the *p*-H_2···HCl complex in comparison to the *o*-H_2···HCl complex.[29] The actual spatial distributions of H_2 and D_2 in complexes with ICl are probably closer to that calculated for H_2 with HCl than the spherical shapes assumed here, but considering the simplistic form of the H_2 + ICl(B,v') utilized in these calculations, we have chosen not to attempt a more accurate depiction of H_2 or D_2.

The full potential surface is averaged over the $I^{35}Cl$(B,v'=3) vibrational level. As a consequence, the intermolecular interactions of D_2 with ICl is reduced to a two-dimensional system, depending only on the center-of-mass separation, R, and the angle between R and the ICl bond, θ, where θ = 0° corresponds to the collinear D_2···ICl orientation. This two-dimensional system was solved in a discrete-variable representation with 120 points in R, evenly spaced between 2 and 26 Å and 50 points in θ that are based on a Gauss−Legendre quadrature grid, the same parameters as were used in our earlier study of H_2···ICl.

The energies of the 25 lowest-energy bound intermolecular vibrational levels are displayed in the right column of Figure 6. Additionally, the probability amplitudes for those levels indicated with letters on the right are shown in Figure 7 in the correspondingly lettered panels. The calculated energies of the levels relative to the D_2 + ICl(B,v'=3) dissociation limit are also indicated below each letter. The probability amplitudes are superimposed on the D_2 + ICl(B,v'=3) PES, and both are plotted as functions of R and θ.

The calculations suggest that the lowest four intermolecular vibrational levels, n' = 0−3, are localized in the well near θ = 100°, and the vibrational motions appear as bending excitations about the asymmetric geometry. Levels at higher energies have probability amplitudes that sample the linear θ = 0° region of the excited-state potential, and most of the features appear as hindered rotor levels of the D_2 about the ICl moiety. There are exceptions, however, as indicated by the nodal patterns in the probability amplitudes included in Figure 7d and f. These probability amplitudes each have radial nodes, suggesting that a stretching motion can accompany the hindered rotor motion. The natures of the different intermolecular vibrational motions are indicated by the different line types in Figure 6; specifically, those excited-state levels that are localized in the well near θ = 100° are depicted as solid, bold lines, levels delocalized in the angular coordinate are thin lines, and levels with intermolecular stretching character are dashed lines.

The energetic region over which the intermolecular vibrational levels remain below the potential barrier for internal rotation is indicated by the red box in Figure 6. Transitions of the ground-state, asymmetric D_2···$I^{35}Cl$(X,v''=0) conformer most likely access the n' = 0 level based on favorable Franck−Condon

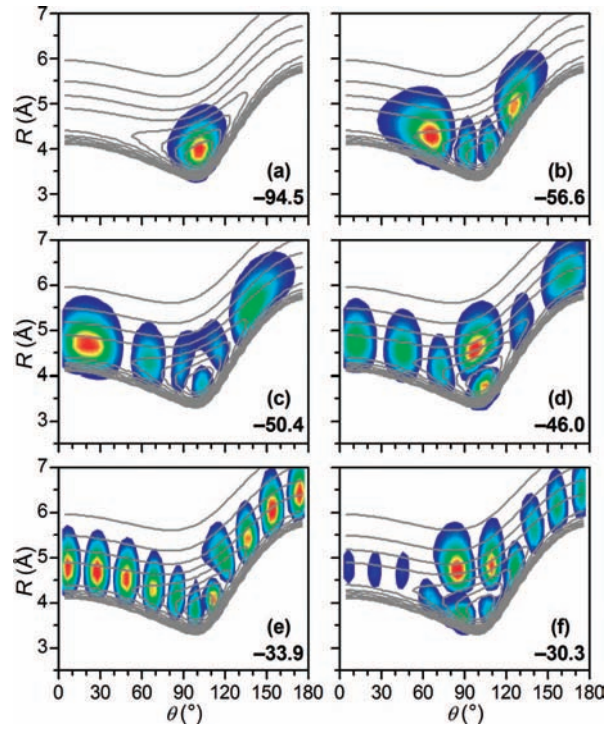

Figure 7. The probability amplitudes for numerous D_2···ICl(B,v'=3) intermolecular vibrational levels with the panel letter associated with the levels identified in Figure 6. The energies of these levels relative to the D_2 + ICl(B,v'=3) dissociation limit are also included. The probability amplitudes are superimposed on the potential energy surface (gray lines), approximated by scaling a He + ICl(B,v'=3) potential.[1] The coordinates represent the D_2 to ICl intermolecular distance, R, and the angle of the D_2 molecule about the ICl bond, θ, with θ = 0° corresponding to D_2 located at the I end of ICl along the ICl axis.

overlap. This band is the lower-energy feature in each spectral region, which has a rotational contour that is nearly the same as that for the corresponding H_2···$I^{35}Cl$ feature characterized in Paper I.[1] The fitting of the rotational contour of the H_2···$I^{35}Cl$ feature revealed nearly the same rigid asymmetric geometries in the ground and excited states. The similarities of the transition energies and rotational contours for the H_2···$I^{35}Cl$ and D_2···$I^{35}Cl$ features support the proposed transitions for this feature.

Although the calculations obtained using the simple scaled potential indicate that there is probability amplitude localized in the θ = 100° region of the PES for excited bending levels up to n' = 3, we expect that the energies of these levels would be sensitive to the details of the intermolecular interactions. On the basis of the energy level diagram for the experimentally observed *p*-D_2···$I^{35}Cl$(B,v'=3) levels, bending levels similar to those calculated are not accessed by transitions of the asymmetric, ground-state conformer. However, spectral features are observed for transitions of the asymmetric *o*-D_2···$I^{35}Cl$(X,v''=0) conformer to two low-lying intermolecular bending levels. Since this complex contains the *o*-D_2 molecule with presumably no rotational angular momentum, j = 0, and spherical symmetry, the interaction of *o*-D_2 with $I^{35}Cl$(B,v'=3) is expected to be more isotropic in the angular coordinate than that for the *p*-D_2(j = 1) + $I^{35}Cl$(B,v'=3) interactions. Correspondingly, the intermolecular bending frequency would be significantly lower for *o*-D_2···$I^{35}Cl$(B,v'=3) than that for *p*-D_2···$I^{35}Cl$(B,v'=3). Thus, it seems reasonable that *o*-D_2···$I^{35}Cl$(B,v'=3) excited intermolecular bending levels may lie below the barrier for internal rotation and have significant

probability amplitude localized in the minimum region of the excited-state PES. The slight asymmetry of the probability amplitude about the minimum of the potential minimum, see for example Figure 7b, will result in a weak but nonzero Franck−Condon overlap between the asymmetric o-$D_2\cdots I^{35}Cl(X,v''=0)$ conformer and these bending levels. The greater than an order of magnitude decrease in intensity of these two spectral features in comparison to the asymmetric band is consistent with this expectation. Note that the binding energy of the p-$H_2\cdots I^{35}Cl(B,v'=3)$ complex, which also has $j = 0$ for the H_2 moiety, is significantly less than that for the deuterated counterpart. The result is that the excited bending levels for this complex would be above the barrier for rotation, and no transitions of the asymmetric p-$H_2\cdots I^{35}Cl(X,v''=0)$ conformer to these bending levels are observed.

Transitions of the C_{2v} $D_2\cdots I^{35}Cl(X,v''=0)$ conformer access higher intermolecular levels that have probability amplitudes sampling the linear region, $\theta = 0°$, of the excited-state potential. Since the energy spacings between these levels are small and are not regular, spectral overlap of the corresponding bands is likely, and definitive assignment of the different levels based on these spectra and model calculations is not possible. While quantitative agreement of the calculated and observed intermolecular vibrational energies is not obtained using the simple scaled potential and has not been attempted, the energy of the barrier to internal rotation seems fairly accurate. The calculations indicate that the highest intermolecular vibrational level that does not sample the linear region is the $n' = 3$ level, which is shown in Figure 7b. Above this energy, the calculated levels resemble hindered rotor levels. This is the same as observed experimentally; only levels accessed by transitions of the C_{2v} ground-state conformer are observed to higher energies than the calculated $n' = 3$ level. The region over which the levels are delocalized and resemble hindered rotor levels is indicated by blue shading in Figure 6.

Details of the radial coordinate of the intermolecular potential are difficult to ascertain without better characterization of the different levels accessed, which is not possible in these experiments. For instance, the first $D_2\cdots I^{35}Cl(B,v'=3)$ intermolecular vibrational level with stretching excitation is calculated to be the $n' = 7$ level, plotted in Figure 7d. Although the radial node is in the minimum region of the potential near $\theta = 110°$ for this level, there is still appreciable probability amplitude in the $\theta = 0°$ region, and transitions of the C_{2v} ground-state conformer could access a stretching level with this character. The first experimentally observed $D_2\cdots I^{35}Cl(B,v'=3)$ level with stretching excitation is ≈ 10 cm^{-1} higher than the $n' = 7$ level. Nevertheless, at these and higher energies, the calculations suggest that levels that are both delocalized in the angular coordinate and have intermolecular stretching excitation exist and can be accessed; this region is indicated by purple shading in Figure 6. Overall, the scaled He + $I^{35}Cl(B,v'=3)$ multidimensional PES has most of the properties necessary to reproduce the general trends of the levels experimentally observed and to justify the observed spectral contributions to transitions of the C_{2v} and asymmetric $H_2\cdots I^{35}Cl(X,v''=0)$ and $D_2\cdots I^{35}Cl(X,v''=0)$ conformers.

4. Summary and Conclusions

The LIF and action spectra of the $D_2\cdots ICl(X,v''=0)$ complexes recorded using varying conditions in the ICl A−X and B−X, $v'-0$ regions, coupled with calculations of the energies and probability amplitudes of the excited-state levels, provide strong evidence that we are observing transitions of two different conformers of the o,p-$D_2\cdots I^{35,37}Cl(X,v''=0)$ van der Waals complex. These conformers most likely correspond to a $D_2\cdots ICl(X,v''=0)$ complex with the D_2 localized at the *I*-atom end of ICl, resulting in an average geometry with C_{2v} symmetry and with an asymmetric structure for which the D_2 subunit is localized in a well orthogonal to the ICl bond axis. The ground-state binding energies, D_0'', are 202(3) and 223.9(2.4) cm^{-1} for the C_{2v} o- and p-$D_2\cdots I^{35}Cl(X,v''=0)$ complexes, respectively. The binding energies of the asymmetric conformers are notably less, 87.7(3)−95.2(2) cm^{-1} for the o-$D_2\cdots I^{35}Cl(X,v''=0)$ complex and 97.3(8)−103.9(3) cm^{-1} for p-$D_2\cdots I^{35}Cl(X,v''=0)$. The equilibrium geometries of the excited-state complexes are also asymmetric, and their binding energies are slightly less than those determined for the asymmetric ground-state conformer.

As expected, because of the increased mass of D_2 over H_2, the $D_2\cdots I^{35}Cl$ complexes are more strongly bound than the corresponding $H_2\cdots I^{35}Cl$ complexes in both the ground and excited electronic states; see Table 2. For the C_{2v} ground-state complexes, the binding energy of p-$D_2\cdots I^{35}Cl(X,v''=0)$ is 20% greater than that of o-$H_2\cdots I^{35}Cl(X,v''=0)$. We compare p-$D_2\cdots I^{35}Cl$ to o-$H_2\cdots I^{35}Cl$ here because both complexes correspond to the H_2/D_2 moiety with $j = 1$ rotational excitation. For the more weakly bound asymmetric conformers, the p-$D_2\cdots I^{35}Cl(X,v''=0)$ binding energy is 9−25% greater than that of o-$H_2\cdots I^{35}Cl(X,v''=0)$, and in the excited state, the difference is similar, 6−26%. The p-$D_2\cdots I^{35}Cl$ and o-$H_2\cdots I^{35}Cl$ complexes are more strongly bound than the o-$D_2\cdots I^{35}Cl$ and p-$H_2\cdots I^{35}Cl$ complexes, which have no rotational angular momentum for the hydrogen moiety, $j = 0$. This trend is consistent with the findings of the Heaven, Lester, and Nesbitt groups and has been attributed to the symmetry of the H_2/D_2 wave function, with the node in the $j = 1$ state serving to enhance the quadrupole interactions of H_2/D_2 with numerous molecular partners.[20,22,27−29] For $H_2\cdots I^{35}Cl$, there was a 19% enhancement in the binding energy of the C_{2v} o-$H_2\cdots I^{35}Cl(X,v''=0)$ complex over that of the C_{2v} p-$H_2\cdots I^{35}Cl(X,v''=0)$ complex. For $D_2\cdots I^{35}Cl$, this enhancement is even less; the C_{2v} p-$D_2\cdots I^{35}Cl(X,v''=0)$ binding energy is only 11% larger than that for C_{2v} o-$D_2\cdots I^{35}Cl(X,v''=0)$.

The results reported here characterizing the o,p-H_2/D_2 + $I^{35,37}Cl$ ground- and excited-state intermolecular PESs should assist in clarifying the role that electrostatic interactions play in long-range interactions and their role in dictating preferred orientations in weakly bound complexes. There are still questions concerning these interactions, especially in the excited states, that high-level calculations may be able to answer. For instance, we have assumed that the D_2 and H_2 molecules behave as spherically symmetric entities. What is the actual role of the hydrogen rotational angular momentum? Perhaps a related question is why are low-lying bending levels observed for the o-$D_2\cdots I^{35}Cl$ conformer but not for any of the other complexes? We are also investigating the role of this rotational angular momentum on the vibrational predissociation dynamics of these species in the excited states.

Acknowledgment. R.A.L. is indebted to the David and Lucile Packard Foundation for a Fellowship in Science and Engineering and to the National Science Foundation for a CAREER Award, CHE-0346745. A.B.M. acknowledges the National Science Foundation CHE-0515627 for funding this work. The authors are indebted to Professor Benjamin McCall (UIUC) for experimental assistance with the preparation of the o-D_2.

References and Notes

(1) Darr, J. P.; Crowther, A. C.; Loomis, R. A.; Ray, S. E.; McCoy, A. B. *J. Phys. Chem. A* **2007**, *111*, 13387.

(2) Boucher, D. S.; Darr, J. P.; Bradke, M. D.; Loomis, R. A.; McCoy, A. B. *Phys. Chem. Chem. Phys.* **2004**, *6*, 5275.

(3) Boucher, D. S.; Strasfeld, D. B.; Loomis, R. A.; Herbert, J. M.; Ray, S. E.; McCoy, A. B. *J. Chem. Phys.* **2005**, *123*, 104312/1.

(4) Strasfeld, D. B.; Darr, J. P.; Loomis, R. A. *Chem. Phys. Lett.* **2004**, *397*, 116.

(5) Boucher, D. S.; Loomis, R. A. *Adv. Chem. Phys.* **2008**, *138*, 375.

(6) McCoy, A. B.; Darr, J. P.; Boucher, D. S.; Winter, P. R.; Bradke, M. D.; Loomis, R. A. *J. Chem. Phys.* **2004**, *120*, 2677.

(7) Bussières, D.; Hoy, A. R. *Can. J. Phys.* **1984**, *62*, 1941.

(8) Coxon, J. A.; Gordon, R. M.; Wickramaaratchi, M. A. *J. Mol. Spectrosc.* **1980**, *79*, 363.

(9) Donovan, R. J.; Ridley, T.; Lawley, K. P.; Wilson, P. J. *Chem. Phys. Lett.* **1993**, *205*, 129.

(10) Takei, T.-A.; Watanabe, A.; Amako, Y. *J. Mol. Spectrosc.* **1995**, *171*, 287.

(11) Bradke, M. D.; Loomis, R. A. *J. Chem. Phys.* **2003**, *118*, 7233.

(12) Boucher, D. S.; Bradke, M. D.; Darr, J. P.; Loomis, R. A. *J. Phys. Chem. A* **2003**, *107*, 6901.

(13) Skene, J. M.; Lester, M. I. *Chem. Phys. Lett.* **1985**, *116*, 93.

(14) Skene, J. M. The Spectroscopy and Dynamics of Iodine Monochloride−Rare Gas van der Waals Compelxes. Ph. D. Thesis, University of Pennsylvania, 1988.

(15) Brown, W. G.; Gibson, G. E. *Phys. Rev.* **1932**, *40*, 529.

(16) Bastida, A.; Zúñiga, J.; Requena, A.; Miguel, B.; Beswick, J. A.; Vigué, J.; Halberstadt, N. *J. Chem. Phys.* **2002**, *116*, 1944.

(17) Darr, J. P.; Crowther, A. C.; Loomis, R. A. *Chem. Phys. Lett.* **2003**, *378*, 359.

(18) Darr, J. P.; Loomis, R. A.; McCoy, A. B. *J. Chem. Phys.* **2005**, *122*, 044318.

(19) Drobits, J. C.; Lester, M. I. *J. Chem. Phys.* **1988**, *88*, 120.

(20) Kaledin, A. L.; Heaven, M. C.; Bowman, J. M. *J. Chem. Phys.* **1999**, *110*, 10380.

(21) Fawzy, W. M.; Kerenskaya, G.; Heaven, M. C. *J. Chem. Phys.* **2005**, *122*, 144318.

(22) Chen, Y.; Heaven, M. C. *J. Chem. Phys.* **1998**, *109*, 5171.

(23) Esposti, A. D.; Werner, H. *J. Chem. Phys.* **1990**, *93*, 3351.

(24) de Leeuw, F. H.; Dymanus, A. *J. Mol. Spectrosc.* **1973**, *48*, 427.

(25) de Jong, W. A.; Styszynski, J.; Visscher, L.; Nieuwpoort, W. C. *J. Chem. Phys.* **1998**, *108*, 5177.

(26) Sadlej, A. J. *J. Chem. Phys.* **1992**, *96*, 2048.

(27) Lovejoy, C. M.; Nelson, D. D., Jr.; Nesbitt, D. J. *J. Chem. Phys.* **1987**, *87*, 5621.

(28) Loomis, R. A.; Lester, M. I. *Annu. Rev. Phys. Chem.* **1997**, *48*, 643.

(29) Anderson, D. T.; Schuder, M.; Nesbitt, D. J. *Chem. Phys.* **1998**, *239*, 253.

(30) Buckingham, A. D. *Discuss. Faraday Soc.* **1965**, *40*, 232.

(31) Ray, S. E.; McCoy, A. B.; Glennon, J. J.; Darr, J. P.; Fesser, E. J.; Lancaster, J. R.; Loomis, R. A. *J. Chem. Phys.* **2006**, *125*, 164314.

(32) Hutson, J. M. *J. Phys. Chem.* **1992**, *96*, 4237.

(33) Han, J.; Heaven, M. C. *J. Chem. Phys.* **2005**, *123*, 064307.

(34) Lovejoy, C. M.; Nesbitt, D. J. *J. Chem. Phys.* **1990**, *93*, 5387.

(35) Chang, B.-C.; Dunlop, J. R.; Williamson, J. M.; Miller, T. A.; Heaven, M. C. *Chem. Phys. Lett.* **1993**, *207*, 62.

(36) Nesbitt, D. J.; Lovejoy, C. M.; Lindeman, T. G.; ONeil, S. V.; Clary, D. C. *J. Chem. Phys.* **1989**, *91*, 722.

(37) Lovejoy, C. M.; Nesbitt, D. J. *Chem. Phys. Lett.* **1988**, *147*, 490.

(38) Loomis, R. A.; Schwartz, R. L.; Lester, M. I. *J. Chem. Phys.* **1996**, *104*, 6984.

(39) Lovejoy, C. M.; Nelson, D. D., Jr.; Nesbitt, D. J. *J. Chem. Phys.* **1988**, *89*, 7180.

JP802917F